

# Microwave radiometry experiment for snow in Altay China: time series of *in situ* data for electromagnetic and physical features of snow pack

Liyun Dai<sup>1</sup>, Tao Che<sup>1,2\*</sup>, Yang Zhang<sup>1</sup>, Zhiguo Ren<sup>1,3</sup>, Junlei Tan<sup>1</sup>, Meerzhan Akynbekkyzy<sup>1</sup>, Lin Xiao<sup>1</sup>, Shengnan Zhou<sup>1</sup>, Yuna Yan<sup>3</sup>, Yan Liu<sup>4</sup>, Hongyi Li<sup>1</sup>, Lifu Wang<sup>5</sup>

<sup>1</sup>Key Laboratory of Remote Sensing of Gansu Province, Heihe Remote Sensing Experimental Research Station, Northwest Institute of Eco-Environment and Resources, Chinese Academy of Sciences, Lanzhou, 730000, China.

<sup>2</sup>Center for Excellence in Tibetan Plateau Earth Sciences, Chinese Academy of Sciences, Beijing, 100101, China.

<sup>3</sup>University of Chinese Academy of Sciences, Beijing, 1000101, China.

<sup>4</sup>Institute of Desert Meteorology, China Meteorological Administration, Urumqi, 830002, China

<sup>5</sup>Altay National Reference Meteorological station, China Meteorological Administration, Altay, 836500, China.

*Correspondence to:* Tao Che (chetao@lzb.ac.cn)

**Abstract.** In this paper, we present a comprehensive experiment, namely, Integrated Microwave Radiometry Campaign for snow (IMCS), in Xinjiang, China, during snow season of 2015/2016. The campaign hosted a dual polarized microwave radiometer operating at L, K and Ka bands to provide minutely passive microwave observations of snow cover at a fixed site, along with daily manual snow pit observation of snow physical parameters, automatic observation of ten-minute 4-component radiation and layered snow temperatures, and meteorological observation of hourly weather data and soil data. To the best of our knowledge, our dataset is unique in providing continuous daily snow pits data and coincident microwave brightness temperatures, radiation and meteorological data, at a fixed site over a full season, which can be straightforwardly used for evaluation and development of microwave radiative transfer models and snow process models, along for land surface process and hydrology models. The consolidated data are available at <http://data.tpdc.ac.cn/zh-hans/data/df1b5edb-daf7-421f-b326-cdb278547eb5/> (doi: 10.11888/Snow.tpdc.270886) (Dai, 2020).

**Key words:** Snow, Microwave radiometry, Snow pit, Experiment

## 1 Introduction

Field experiments/campaigns, as the main and most important approach for snow studies, have been conducted to obtain the electromagnetic and physical characteristics of snow cover. The main experiments/campaigns are summarized in table 1. The Cold Land Processes Field Experiment (CLPX) (<https://nsidc.org/data/clpx/index.html>), one of the most well-known experiments, was carried out from winter of 2002 to spring of 2003 in Colorado, USA (Cline et al., 2003). During the campaign, snow pits

39 were collected to coincide with airborne and ground remote sensing observations. In 2017, NASA  
 40 SnowEx campaign (<https://nsidc.org/data/snowex>) was conducted in Colorado to test and develop  
 41 algorithms for measurement of SWE in forested and non-forested areas by providing multi-sensor  
 42 observations of seasonally snow-covered landscapes (Brucker et al., 2017). The campaign is still ongoing  
 43 and will be conducted in other areas with different snow conditions. In northern Canada, mobile sled-  
 44 mounted microwave radiometers were deployed in forest, open and lake environments from November  
 45 2009 to April 2010 and snow characteristics within the footprints of radiometers were measured to  
 46 improve the understanding of the influence of snow characteristics on brightness temperatures (Derksen  
 47 et al., 2012; Roy et al., 2013). The aforementioned microwave experiments were conducted at different  
 48 sites for different land cover, resulting in good representativity for evaluating snow microwave emission  
 49 model (Tedesco and Kim, 2006; Royer et al., 2017), however, with relative short temporal range, while  
 50 dense temporal resolution is important to reveal the evolution of snow characteristics.

51 In the Arctic region, the Nordic Snow Radar Experiment (NoSREx) campaign was conducted at a  
 52 fixed field of the Arctic boreal forest area in Sodankylä, Finland, during 2009 ~ 2013 (Lemmetyinen et  
 53 al., 2016). The experiment provided a continuous time series of active and passive microwave  
 54 observations of snow cover spanning an entire winter season, with synchronous observations of snow pit  
 55 weekly. In Asia, an experiment of radiation budget over snow cover (JERBES) was conducted in Japan.  
 56 In the experiment, snow pit work at 3 or 4 day intervals was conducted simultaneously with radiation  
 57 budget observations during winter of 1999/2000 and 2000/2001 to analyze the effects of snow physical  
 58 parameters on albedo (Aoki et al., 2003). The NoSREx and JERBES experiments, for fixed field  
 59 observation, provided improved time series of data than CLPX and SnowEx. Weekly observation could  
 60 reflect general evolution process of snow characteristics but might miss some key details that occur at  
 61 sub-weekly scales. In the Tibetan plateau with shallow snow cover, multiple years of microwave  
 62 radiometry observation at L band were conducted to study passive microwave remote sensing of frozen  
 63 soil (Zheng et al., 2019 and 2021; Zhang et al., 2021). However, in the long-term series of experiment,  
 64 no snow pit was measured and the microwave radiometry observation was only performed at L band  
 65 which is insensitive to snowpack.

66 **Table 1. Summary of existing experiments for microwave and optical radiation and physical features of**  
 67 **snowpack**

Campaign	Location	Temporal range	Observation content
CLPX	Different sites in Colorado,	February and March of 2002 and 2003	Inconsecutive multiple sensor observation, including microwave radiometry over snow, and synchronous snow pit measurements at different sites with short temporal range
SnowEx-year 1	Grand Mesa, and Senator Beck Basin, Colorado	February of 2017	Inconsecutive multiple sensor observation, including microwave radiometry over snow, and synchronous snow pit measurements at different sites with short temporal range
CMRES <sup>1</sup>	Mobile observation at Forest, open and lake	November of 2009-April of 2010	Mobile microwave radiometry and snow pit observation within footprint of radiometer. Short temporal range and inconsecutive observation

---

	in the northern Canadian region		
NoSREx	Fixed site in Sodankylä, Finland	Snow season during 2009- 2013	Consecutive microwave radiometry and SAR observation over snow, and weekly snow pit measurement
JERBS	Fixed site in Japan	Snow season during 1999- 2000	Consecutive optical radiation observation over snow and consecutive snow pit measurement at 3 or 4-day interval
IMCS (Presented in this work)	Fixed site in China	November of 2015-March of 2016	Consecutive microwave radiometry and optical radiation observation, and consecutive daily snow pit measurements

---

68 Note: <sup>1</sup>CMRES: Microwave radiometry experiment on snow cover conducted in northern Canada

69

70 To understand the evolution of snow characteristics and their influence on passive microwave  
71 brightness temperatures and radiation budget, an integrated field experiment on snowpack was conducted  
72 during a full snow season, in Altay, China. The experiment was designed to cover periods from snow-  
73 free conditions to eventual snow melt-off during 2015/2016. The microwave radiometry measurements  
74 at L, K and Ka bands for multiple angles were complemented by a dual-polarized microwave radiometer  
75 with 4-component radiation and daily in situ observations of snow, soil and atmospheric properties, using  
76 both manual and automated methods. To the best of our knowledge, our dataset is unique in providing  
77 continuous daily snow pit observations over a full snow season at a fixed site, along with synchronous  
78 microwave brightness temperatures, radiation and meteorological data. The dataset is consolidated and  
79 organized, which can be easily used for other researchers with interests.

80 In the next section, the experiment location, parameters, and parameter measurement protocols are  
81 described. Section 3 introduces the consolidated data that was released at the National Tibetan Plateau  
82 Data Center, China, which provides data support for international science programs (Li et al., 2021; Pan  
83 et al., 2021). Section 4 presents content of brightness temperature, 4-component radiation, snow pit data,  
84 soil temperature and moisture, and meteorological data. Section 5 discusses the possible applications and  
85 uncertainties. Finally, the conclusions are summarized in section 6.

## 86 **2 Description of experiment setup**

### 87 **2.1 Measurement location**

88 The Integrated Microwave Radiometry Campaign for snow (IMCS) was performed during the  
89 2015/2016 snow season (from November 27, 2015 to March 25, 2016) at the Altay National Reference  
90 Meteorological station (ANRMS) (N47°44'26.58", E 88°4'21.55"), which is approximately 6 km from  
91 the foot of Altay mountain in the northwest China (Figure 1). Altay mountain with elevation up to 3000  
92 m, running northwest and southeast, is at the junction of China, Russia, Mongolia and Kazakhstan,  
93 providing snow water resources for these four countries. The average annual maximum snow depth  
94 measured in this station is approximately 40 cm, with a maximum over 70 cm. In the southwest of Altay  
95 mountain, crop land and desert with flat terrain are the dominant land covers. Snow cover is critical fresh

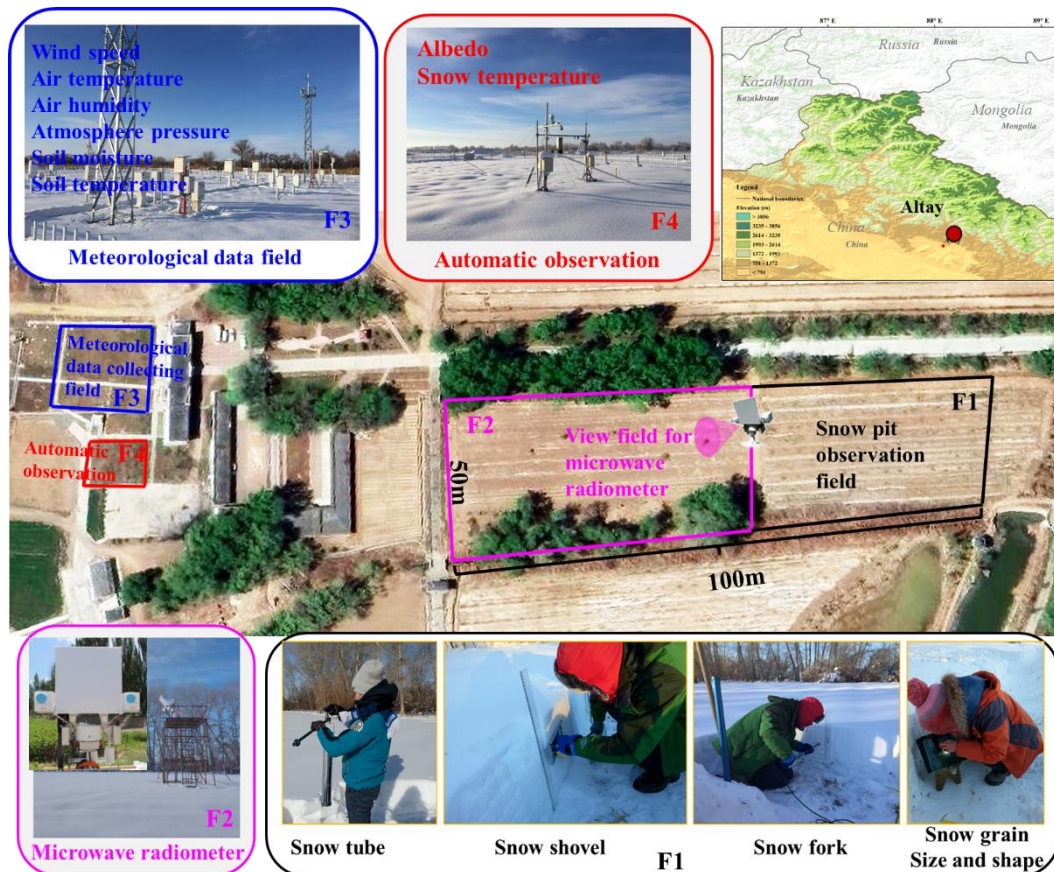
96 water for the irrigation in this area. In this experiment, measurements included microwave radiometry,  
97 4-component radiation, snow pit and soil parameters. The test sites of this experiment were four  
98 neighboring bare rectangle fields in the ANRMS with areas of 2000 m<sup>2</sup> (Field1 (F1) in Figure 1), 3000  
99 m<sup>2</sup> (Field 2 (F2) in Figure 1), 400 m<sup>2</sup> (Field3 (F3) in Figure 1) and 300 m<sup>2</sup> (Field4 (F4) in Figure 1),  
100 respectively.

101 In the F2, the ground-based microwave radiometer was set up in the middle of the field, facing south  
102 to collect brightness temperatures over snow cover. F1 behind the microwave radiometers (north of the  
103 radiometers) was for manual snow pit data collection. The microwave radiometer observations and snow  
104 pit data collections were conducted by Northwest Institute of Eco-Environment and Resources, Chinese  
105 Academy of Science (NIEER) from November 27, 2015 to March 25, 2016 (snow free after March 25,  
106 2016).

107 F3 was for meteorological measurements including wind speed, wind direction, air temperature, air  
108 wetness, air pressure, precipitation, soil temperature, soil moisture among others. These parameters were  
109 automatically obtained from instruments, and the instruments setup and data collection were operated by  
110 ANRMS. In this experiment, we requested the wind, air pressure, air wetness, air pressure, soil  
111 temperature and moisture data during this experiment from ANRMS. F4 was designed for automatic  
112 measurement of layered snow temperatures, snow density, SWE, snow depth, and albedo, with  
113 instruments operated by NIEER since 2013. However, during the experiment, the instruments for snow  
114 density and SWE were not functional, and we only collected layered snow temperatures and 4-component  
115 radiation.

116 Because the four observation fields, located within the domain of the station, are with distance less  
117 than 100 m, it is reasonable to assume that the snow characteristics and soil and weather conditions are  
118 consistent among these four fields.

119



120

121 **Figure 1.** Location of the Altay National Reference Meteorological station (ANRMS) in Asia, along with the  
 122 four test sites in the ANRMS. F1 (approximately 40 m × 50 m) was for snow layering, layer thickness, snow  
 123 density, snow grain size and shape of each layer. F2 (approximately 60 m × 50 m) was for microwave  
 124 radiometers observations. F3 was for meteorological and soil data collection operated by the ANRMS. F4 was  
 125 for the automatically observation of the snow temperature, and 4-component radiation, designed by  
 126 Northwest Institute of Eco-Environment and Resources, Chinese Academy of Science (NIEER).

127 **2.2 Measurement methods**

128 The microwave signatures from snowpack vary with snow characteristics, soil and weather  
 129 conditions. In this experiment, the measurements include microwave radiometry observation to collect  
 130 brightness temperature, manual snow pit observation to collect snow physical parameters, automatic  
 131 observation to collect 4-component radiation and snow temperatures, and meteorological observation  
 132 containing weather data and soil data.

133 **2.2.1. Microwave radiometry**

134 The brightness temperatures at 1.4 GHz, 18.6 GHz, and 36.5 GHz for both polarization (Tb1h, Tb1v,  
 135 Tb18h, Tb18v, Tb36h, Tb36v) were automatically collected using a six-channel dual polarized  
 136 microwave radiometer RPG-6CH-DP (Radiometer Physics GmbH, Germany,  
 137 <https://www.radiometerphysics.de/products/microwave-remote-sensing-instruments/radiometers/>). The  
 138 technical specifications of the RPG-6CH-DP are described in Table 2. The RPG-6CH-DP contains a  
 139 built-in temperature sensor used for measuring air temperature. The automated data collection frequency  
 140 was set to 1 minute.

141

142

**Table 2. Technical Specifications of the RPG-6CH -DP Microwave Radiometer.**

Parameter	Value
Manufacturer	Radiometer Physics GmbH
System noise temperatures	<900 K
Bandwidth	400MHz (20MHz for 1.4 GHz)
System stability	0.5 K
Dynamic range	0~400 K
Frequencies (GHz)	1.4, 18.7, 36.5
Polarizations	V, H
Internal calibration	Internal Dicke switch and software control for automatic sky tilt calibration
Receiver and antenna thermal stabilization	< 0.015 K
Antenna sidelobe level	< -30 dBc
Optical resolution (HPBW)	6.1° (11° for 1.4 GHz)
Incidence angle	0~90°
Azimuth angle	360°

143

144

145

146

147

148

149

150

151

152

153

154

155

156

157

158

159

160

Before the snow season, a platform with height of 5 m, length of 4 m and width of 2 m was constructed in the experiment field (Figure 2). A 4-m orbit was fixed on the platform. The RPG-6CH-DP was set up on the orbit and could be moved along the orbit. The microwave radiometers at K and Ka bands began working from November 27, 2015, while the L band radiometer began working since January 30, 2016. These radiometers were sky tipping calibrated, with accuracy of 1 K. In clear sky conditions, the sky brightness temperatures were approximately  $29.7 \pm 0.3$  K at 18.7 GHz and  $29.3 \pm 0.9$  K at 36.5 GHz for both polarizations. While the sky brightness temperatures at L band showed large fluctuation. They ranged from -1 to 8 K for horizontal polarization, and 1 to 16 K for vertical polarization.

Generally, the radiometers were fixed in the middle of the orbit to observe snow cover with incidence angle of 50°. Multi-angle observations were conducted after every big snowfall, or every 5 days in the stable period. In the melt period, observation frequency increased. There are total seventeen multi-angle observation on December 3, 19, and 30; January 3, 8, 13, 18, 3, and 28; February 3; March 3, 10, 15, 22, 26, 28, and 31, when the radiometer was set to scan the ground at different incidence angles at the left, middle and right of the orbit, respectively. Although the view fields of the antennas for 1.4 GHz, 18.7 GHz and 36.5 GHz did not completely overlap, the measured results showed that the brightness temperatures observed at the left, middle and right of the orbit varied within 1 K. Therefore, the snow and soil conditions were considered homogeneous within the view fields of the three antennas.

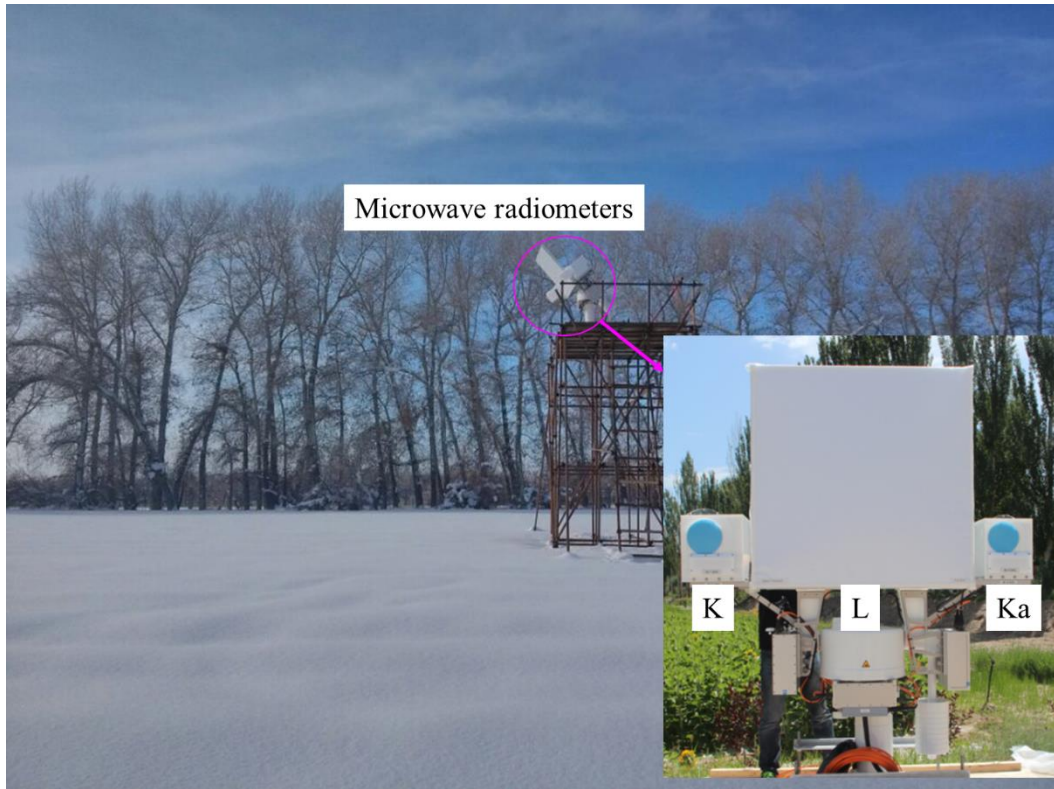


Figure 2. Ground-based microwave radiometer observation system.

### 2.2.2 Snow pit measurement

The snow characteristics, including snow layering, snow layer thickness, grain size, snow density, and snow temperature, were collected by manual snow pit measurements in the black field. These data were daily collected during 8:00-10:00 am local time, from November 27, 2015 to March 25, 2016, except 7 days (please see Table 3). Although the snow temperatures were manually measured at snow pits, the automatically collected snow temperatures in the red field were utilized in this study, because the temperature measured at snow pits could not reflect the natural temperature profile when the snow pits exposed to air.

Table 3. Variables collected by manual daily snow pit measurement in black field in figure 1, along with their observation instruments, observation time and frequencies.

Parameter	Instruments	Precision	Layering style	Observation time or frequency	Absent date
Layer thickness (cm)	Ruler	0.1cm	Natural layering	local time	no
Snow density (g/cm <sup>3</sup> )	Snow tube (Chinese Meteorological Administration)	pressure: 0.1g/cm <sup>2</sup> , snow depth: 0.1 cm	Whole snowpack	8:00-10:00 am	no
Snow density (g/cm <sup>3</sup> )	Snow shovel (NIEER)	weight: 0.01g, volume: 1cm <sup>3</sup>	Every 10 cm		January 2-3, 2016;



Snow density (g/cm <sup>3</sup> ) and	Snow fork (Toikka Engineering Ltd.)	0.0001g/cm <sup>3</sup>	Every 5 cm	February 20, 2016
Liquid water content (%)	Snow fork	0.001%	Every 5 cm	
Snow grain size (mm)	Anyty V500IR/UV	0.001mm	Natural layering	December 24, 31, 2015;
Snow grain shape	Shape card	N/A	Natural layering	January 1- 3, 23, 2016, February 20, 2016

175

176

177

178

179

180

181

182

183

184

185

186

187

188

189

190

191

192

193

194

195

196

197

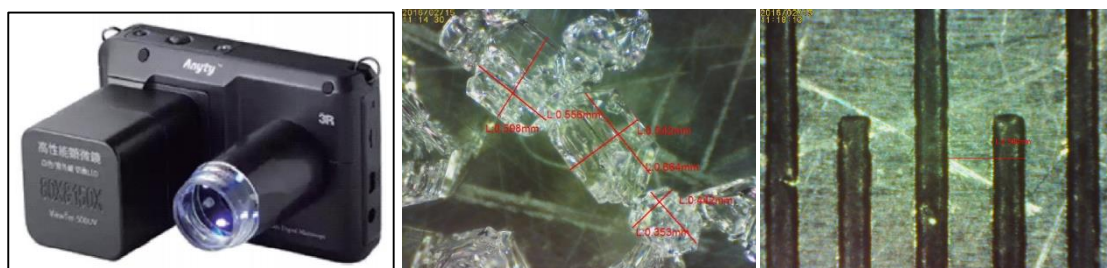
198

199

The first step of snow pit measurement is making a snow pit. In the black field, a new snow pit was dug each day using a spade. The snow pit was approximately 2 m x 1m to make sure all parameters could be measured from unbroken snowpack. The snow pit section was made as flat as possible using a flat shovel or ruler. When the snow profile is exposed to air for a long time, the snow characteristics will be influenced by environment and will be different from the natural snow characteristics. In order to make sure every observation conducted on natural snow pit, the snow pit was backfilled with the shoveled snow after finishing all observations, and the new snow pit in the following day was made at least 1-m distance away from the latest snow pit. After finishing a snow pit, the natural snowpack stratification was then visually determined, and the thickness of each layer was recorded against a ruler.

The next step was measuring grain size and shape type in each layer. The grain size and type within each natural layer were estimated visually using a microscope with an “Anyty V500IR/UV” camera (Figure 3a). The software “VIEWTER Plus” matched the microscope was used to measure grain size. The grain type was determined based on Fierz et al. (2009). In this experiment, we utilized the length of longest axes and the length of shortest axes to describe grain size (Figure 3b). When using the software to measure the grain size, a reference must be needed. In this experiment, a ruler marked 0.5 mm was used as a reference (Figure 3c). We adjusted the focus of the camera to make sure the grains at the clearest status in camera to take photos, and the photo of ruler scale was taken at the same focus. If the thickness of one layer was less than 10 cm, measurements were performed at the top and bottom of the layer, respectively. If the thickness was greater than 10 cm, measurements were performed at the top, middle, and bottom of the layer, respectively. For each layer, at least 5 photos were taken, and the longest axes length and the shortest axes length of at least 10 typical grains were recorded. The final grain size was the average of the 10-group recorded values. Figure A1 presents an example of the original photos of grains in each layer, and Table A1 shows the matched record of longest and shortest axis length.

200

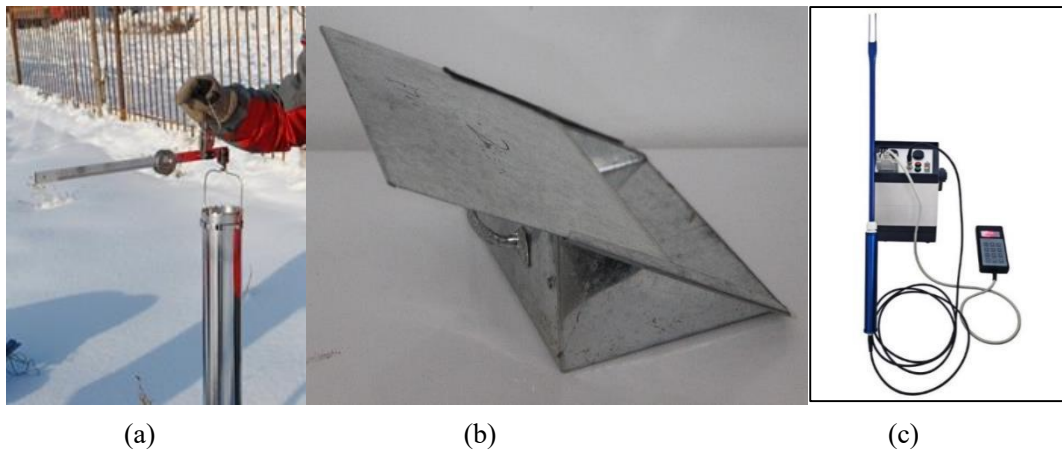




201  
202  
203  
204  
205  
206  
207  
208  
209  
210  
211  
212  
213  
214  
215  
216  
217  
218

(a) (b) (c)  
**Figure 3. (a) Picture of microscope “Anyty V500IR/UV”, (b) the measured longest axes lengths and shortest axes length of particles, and (c) the reference ruler scale.**

Snow density was measured using three instruments: snow tube, snow shovel and snow fork (Figure 4). The snow tube instrument, designed by Chinese Meteorological administration, contains a metal tube with the base area of 100 cm<sup>2</sup> and the length of 60 cm, and a balance (figure 4a). It was utilized to measure the snow density of a whole snowpack by weighing the snow sample. The snow shovel is a 1500 cm<sup>3</sup> wedge-type sampler, and its length, width and height are 20 cm, 15 cm, and 10 cm, respectively (figure 4b). It was utilized to measure snow density every 10 cm (0-10 cm, 10-20 cm, 20-30 cm...). The snow fork (figure 4c) is a microwave resonator that measures the complex dielectric constant of snow, and adopts a semi-empirical equation to estimate snow density and liquid water content based on the complex dielectric. It was utilized to measure snow density and liquid water content at 5-cm intervals starting 5 cm above the snow/soil interface (5cm, 10cm, 15 cm, 20cm...). In order to decrease the observation error, every measurement repeated three times. If there was an abnormal value, a fourth measurement would be performed to ensure the accuracy. Table A2 is an example record table for snow density. The average value of the three-time observation was the final value.



219  
220  
221  
222

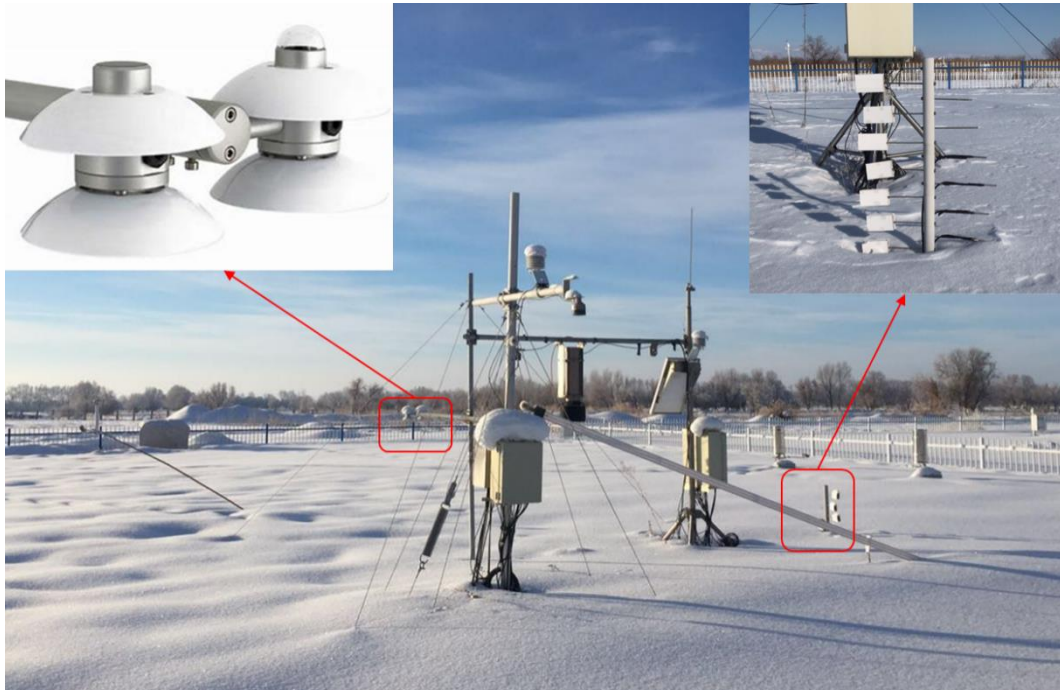
(a) (b) (c)  
**Figure 4. Three instruments for snow density: (a) Snow tube, (b) Snow shovel, and (c) Snow fork.**

### 2.2.3 Automatic radiation and temperature measurement

224  
225  
226  
227  
228  
229  
230  
231  
232  
233

In the red field, the 4-component radiation was automatically measured by Component Net Radiometer (NR01) manufactured by Hukseflux, and layered snow temperatures was measured by Campbell 109S temperature sensors, respectively. The temperature sensors were set up on a vertical pole inserted in soil (Figure 5). The sensors' heights are 0 cm, 5 cm, 10 cm, 15 cm, 25 cm, 35 cm, 45 cm, and 55 cm above soil/snow interface, and temperatures were collected every ten minute.

The NR01 net radiometer was set up to measure the energy balance between incoming short-wave and long-wave far infrared radiation versus surface-reflected short-wave and outgoing long-wave radiation. The range of short wave is 285~3000nm, and the range of long wave is 4.5~40 um. The 4-component radiation was automatically recorded every ten minutes. In addition, the sensor was equipped with a Pt100 temperature sensor for parallel recording of the sensor temperature.



234

235

**Figure 5. Set up of temperature sensors and CNR01 in the red field.**

236

237

#### **2.2.4 Meteorological observation**

238

The meteorological data include air temperature, air pressure and humidity, wind speed, soil temperature at -5 cm, -10 cm, -15 cm and -20 cm, and soil moisture at -10 cm and -20 cm. These parameters are routine observations conducted at ANRMS. The instruments used for soil and weather parameters observations are produced by China Huayun Meteorological Technology Group Corporation.

239

240

241

242

**Table 4. Automatically observed variables and the observation instruments, observation time and frequencies.**

244

Parameter	Instruments	Precision	Layering style	Observation time or frequency
Snow temperature(°C)	Temperature sensors (Campbell 109S)	0.001 °C	0 cm, 5 cm, 10 cm, 15 cm, 25 cm, 35 cm, 45 cm, and 55 cm	Ten-minute
4-component radiation (W/m <sup>2</sup> )	Component Net Radiometer NR01 (Hukseflux)	0.001 W/m <sup>2</sup>	6 feet above ground	Ten-minute
Soil temperature (°C)	Soil temperature sensor (China Huayun)	0.1 °C	-5cm, -10 cm, -15cm and -20 cm	Hourly
Soil moisture (%)	Soil moisture sensor (DZN3, China Huayun)	0.1%	-10 cm and -20 cm	Hourly
Air temperature (°C)	Thermometer screen (China Huayun)	0.1 °C	6 feet above ground	Hourly

Air pressure (hPa)	Thermometer screen (China Huayun)	0.1 hPa	6 feet above ground	Hourly
Air humidity (%)	Thermometer screen(China Huayun)	1%	6 feet above ground	Hourly
Wind speed (m/s)	Wind sensor(China Huayun)	0.1m/s	10 m above ground	Hourly

245

246 The air temperature, pressure and humidity were collected using temperature and wetness sensor in  
 247 thermometer screen. The wind speed and direction were measured using wind sensor set up at 10 m on  
 248 a tower. Soil moisture and temperature were automatically measured using moisture sensor and  
 249 temperature sensor. Figure 6 depicts the instruments for these observations.



250

(a)

(b)

(c)

(d)

251

252 **Figure 6. Instruments for observation of (a) air temperature and wetness, (b) wind speed, (c) soil temperature**  
 253 **and (d) soil moisture.**

### 254 3 Description of consolidated IMCS dataset

255 The microwave brightness temperature, snow parameters, meteorological data were recorded in  
 256 different formats, and their observation frequencies and times were different. These data must be  
 257 reorganized and consolidated for ease of use. The values from the three-time measurements for snow  
 258 density in each layer were averaged to obtain the final snow density. The length of the longest and shortest  
 259 axes of particles in each photo were measured using the software. The average lengths of longest and  
 260 shortest axes from all photos in each layer were obtained as the final grain size. The daily snow pit data  
 261 were finally consolidated into a NetCDF file “snow pit data.nc”.

262 The time series of automated layered snow temperature and 4-component radiation data were first  
 263 processed by removal of abnormal values and gap fill, and then consolidated into a NetCDF file “ten-  
 264 minute 4 component radiation and snow temperature.nc”. The ground-based brightness temperatures and  
 265 the formatted weather and soil data requested from ANRMS were provided ‘as is’. Brightness  
 266 temperature data were divided into time series of brightness temperature and multi-angle brightness  
 267 temperatures, and separately stored in two NetCDF files. The weather and soil data were consolidated  
 268 into a NetCDF file “hourly meteorological and soil data.nc”. Table 3 describes the contents of the  
 269 provided dataset.

#### 270 1) Brightness temperatures data:

271 Minutely brightness temperature at 1.4 GHz, 18 GHz and 36 GHz for both polarizations at incidence  
 272 angle of 50°. This data include time, incidence angle, azimuth angle, and brightness temperatures at the  
 273 three bands for both polarizations.

274 Seventeen groups of calibrated brightness temperature at 1.4 GHz, 18.7 GHz and 36.5 GHz for both  
 275 polarizations at different incidence angles (30, 35, 40, 45, 50, 55, 60°). This data include time, incidence  
 276 angles, azimuth angle, and brightness temperatures at the three bands for both polarizations.

277 **2) Manual snow pit data:**

278 Daily snow pit data include date, snow depth, layered snow thickness, average longest axis, average  
 279 shortest axis, grain shapes of each layer; layered snow density using snow fork (snow density at different  
 280 heights, such as SF\_5cm, SF\_10cm, SF\_15cm), snow density using snow tube, layered snow density  
 281 using snow shovel (such as SS\_0-10cm, SS\_10-20cm, SS\_20-30cm, SS\_30-40cm).

282 **3) Automated snow temperature and radiation data**

283 Ten-minute 4-component radiation and snow temperature data include time, short-wave incident  
 284 radiation, short-wave reflected radiation, long-wave infrared incident radiation, long-wave infrared  
 285 reflected radiation, sensor temperature, and snow temperatures at different heights (such as ST\_0cm,  
 286 ST\_5cm)

287 **4) Meteorological and soil data:**

288 Hourly weather data include time, air temperature, pressure, humidity, wind speed, soil temperature  
 289 at 5 cm, 10 cm, 15 cm and 20 cm, and soil moisture at 10 cm and 20 cm.

290

291 **Table 3. Description of consolidated data**

Data	Content	File name	Variables
Brightness temperature	Brightness temperature	TBdata.nc	Time (yyyy-mm-dd hh:mm:ss), Tb1h, Tb1v, Tb18h, Tb18v, Tb36h, Tb36v, incidence angle, azimuth angle
	Multi-angle brightness temperatures	TBdata-multiangle.nc	Time (yyyy-mm-dd hh:mm:ss) , Tb1h, Tb1v, Tb18h, Tb18v, Tb36h, Tb36v, incidence angle, azimuth angle
Manual snow pit data	Layer thickness, layered grain size and shape, snow density	Daily snow pit data.nc	Time (yyyy-mm-dd), snow depth, th1, Lg1, Sg1, th2, Lg2, Sg2,th3, Lg3, Sg3, th4, Lg4, Sg4, th5, Lg5, Sg5, th6, Lg6, Sg6, Stube, SS_0-10, SS_10-20, SS_20-30, SS_30-40, SS_40-50, SF_5, SF_10, SF_15, SF_20, SF_25, SF_30, SF_35, SF_40, SF_45, SF_50, shape1, shape2, shape3, shape4, shape5, shape5
Automated snow temperature and radiation data	4-component radiation, snow temperature	Ten-minute 4 component radiation and snow temperature.nc	Time (yyyy-mm-dd hh:mm), SR_DOWN, SR_UP, LR_DOWN, LR_UP, T_Sensor, ST_0cm, ST_5cm, ST_15cm, ST_25cm, ST_35cm, ST_45cm, ST_55cm
Meteorological and soil data	meteorological data, soil moisture and temperature	Hourly meteorological and soil data.nc	Time (yyyy-mm-dd hh), Tair, Wair, Pair, Win, SM_10cm, SM_20cm, Tsoil_5cm, Tsoil_10cm, Tsoil_15 cm, Tsoil_20cm

292 Note: th: snow thickness, Lg: long axis, Sg: short axis, shape: grain shape;

293 Stube: snow density observed using snow tube, SS: snow density observed using snow shovel, SF: snow density

294 observed using snow fork; ST: snow temperature; SR\_DOWN: downward short-wave radiation, SR\_UP: upward

295 short-wave radiation, LR\_DOWN, downward long-wave radiation, LR\_UP: upward long-wave radiation, T\_sensor:  
 296 sensor temperature; Tair: air temperature, Wair: air wetness, Pair: air pressure, Win: wind speed.

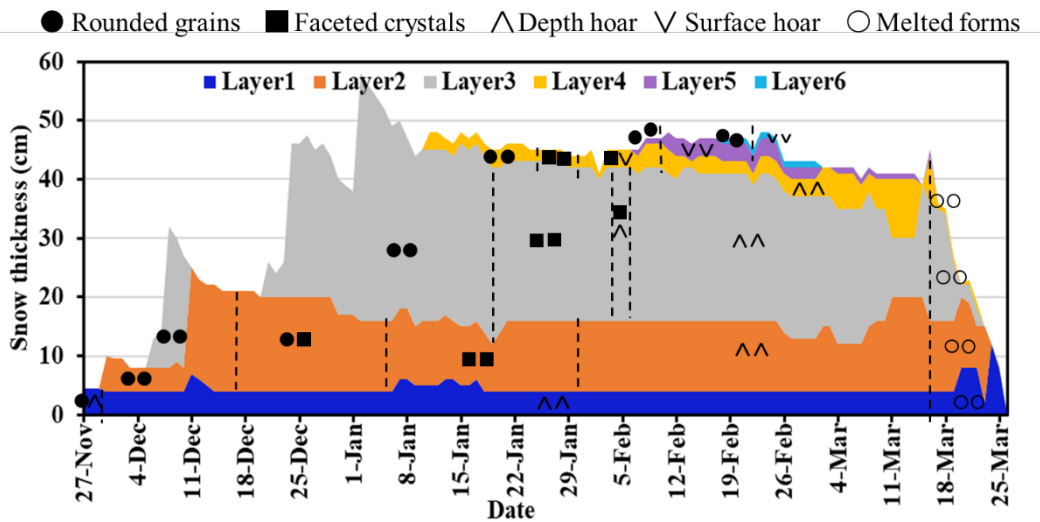
297 **4 Overview and preliminary analysis of collected data from IMCS**

298 **4.1 Snow characteristics**

299 **4.1.1 Layering grain size and grain shape**

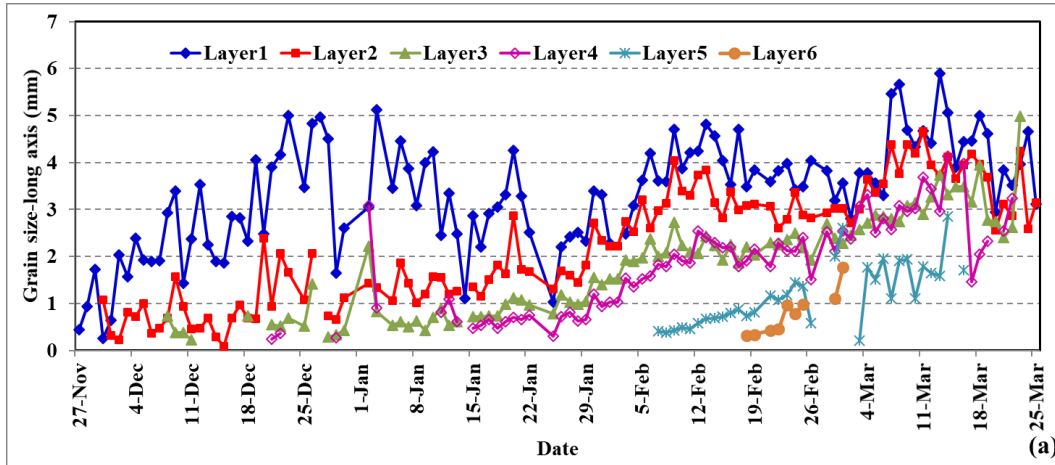
300 During 2015/2016, snow cover began on November 25, 2015, and ended on March 25, 2016. During  
 301 this snow season, there were seven snowfall events and each formed a distinct snow layer except for the  
 302 third event whose layering was indistinguishable from the second layer (Figure 7 gray). The fourth event  
 303 was the biggest. After, the snow depth started to decrease and the snow density increased. Snow cover  
 304 began melting on March 14 and ended within 10 days.

305 Grain sizes within all layers increased during the snow season, except in the bottom layer where  
 306 grain size experienced a decrease from December 28 to January 20 (Figure 8). In the vertical profile,  
 307 grain size increased from top to bottom with the snow age. The grain size of the fresh snow was  
 308 approximately 0.3 mm during the experiment. The biggest long and short axis, occurring in Layer 1  
 309 during the melt period, were up to 6 cm and 4 cm, respectively. The length of short axes is approximately  
 310 0.7 of the length of long axes. The grain shape generally developed from rounded grains to facet crystals,  
 311 and then to depth hoar. After March 13, 2016, the minimum air temperature increased to above 0°C,  
 312 snowmelt accelerated, and the grain shape developed to melted forms (Figure 7).  
 313

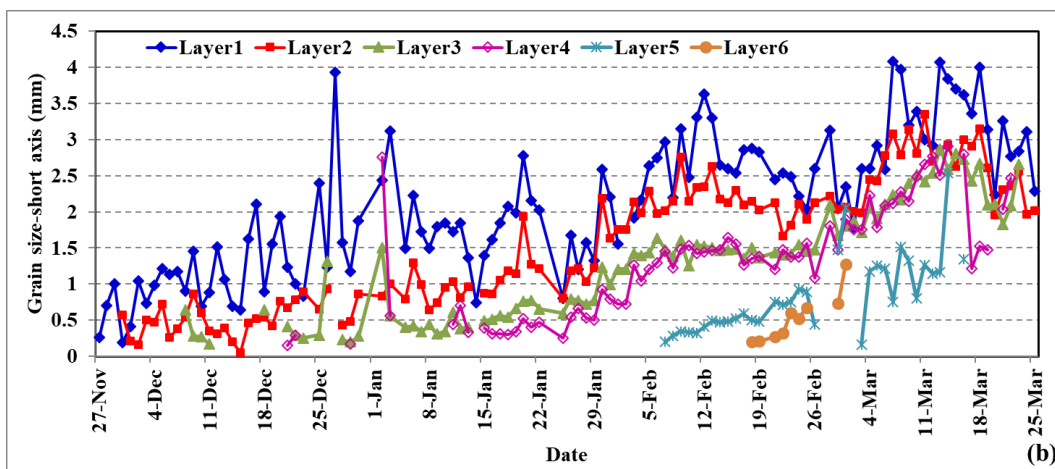


314  
 315 **Figure 7. Daily variation in snow layers and grain shape in each layer from November 27, 2015 to March 25,**  
 316 **2016.**





317



318

319 **Figure 8.** Daily variation in grain size within each layer from November 27, 2015 to March 25, 2016. The layer  
 320 thicknesses are presented in figure 7.

321

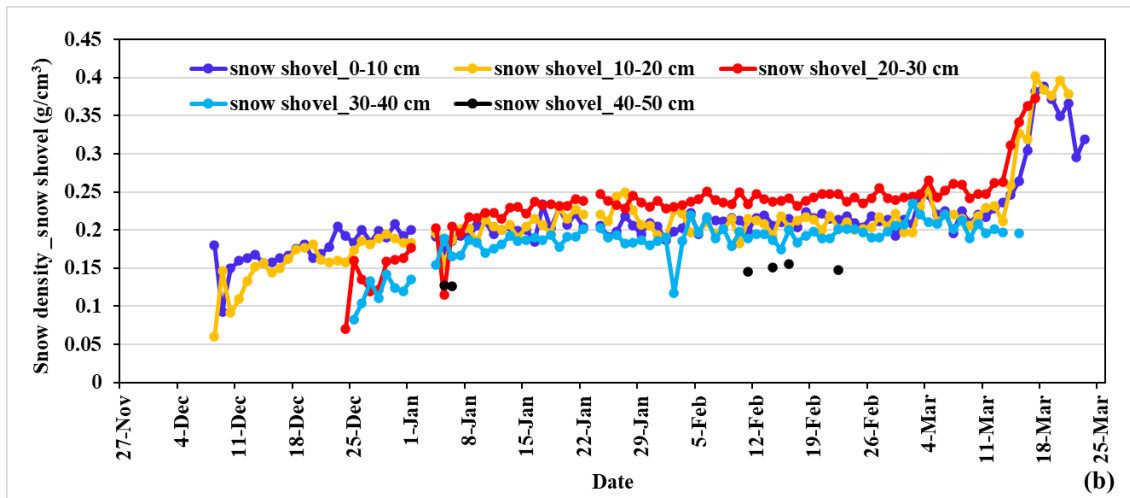
322 **4.1.2 Snow density**

323 Snow density measured by three different instruments shows that the density of fresh snow ranged  
 324 between 0.05~1.0 g/cm<sup>3</sup> (Figure 9). The snow densities increased with snow age, and remained stable  
 325 after reaching ~0.2-0.25 g/cm<sup>3</sup>. From March 14 on, snow densities abruptly increased, with the maximum  
 326 value over 0.45 g/cm<sup>3</sup>. In the vertical profile, snow density increased from top to bottom in the  
 327 accumulation phase. However, after January 3, 2016, snow densities in the middle layers were larger  
 328 than those in the bottom and upper layers due to the well-developed depth hoar of bottom layer. In the  
 329 melting phase, there were no significant different for the snow densities in all layers. Snow fork provided  
 330 most detail snow density profile, but systematically underestimated snow density compared with snow  
 331 tube and snow shovel by 24% (Dai et al., 2022).

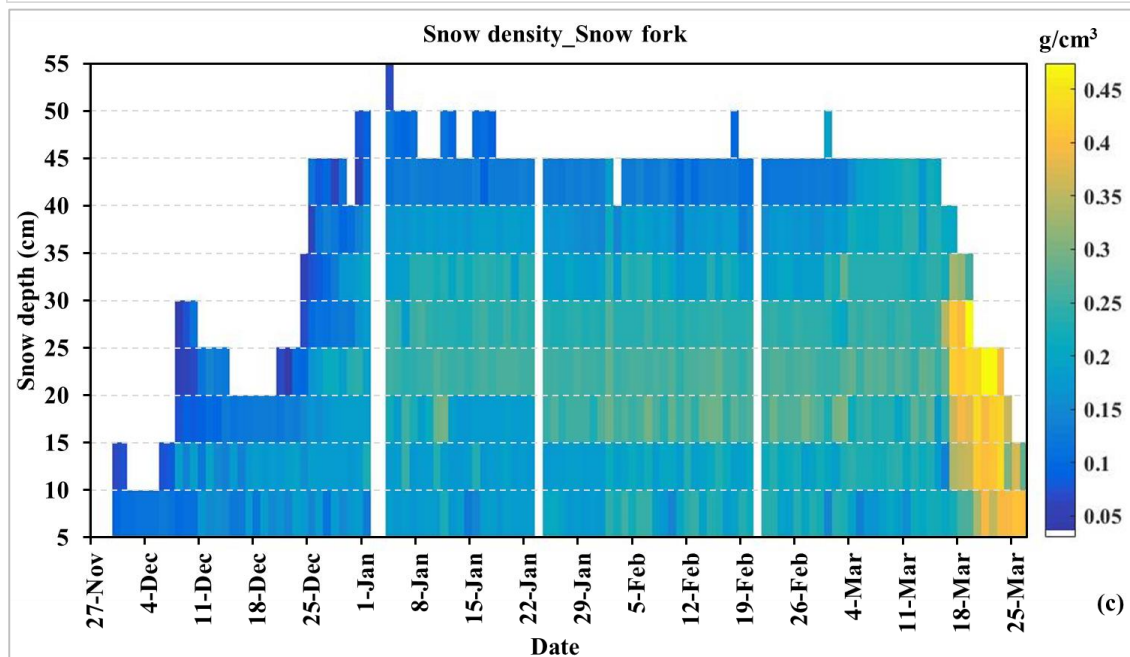




332



333



334

335

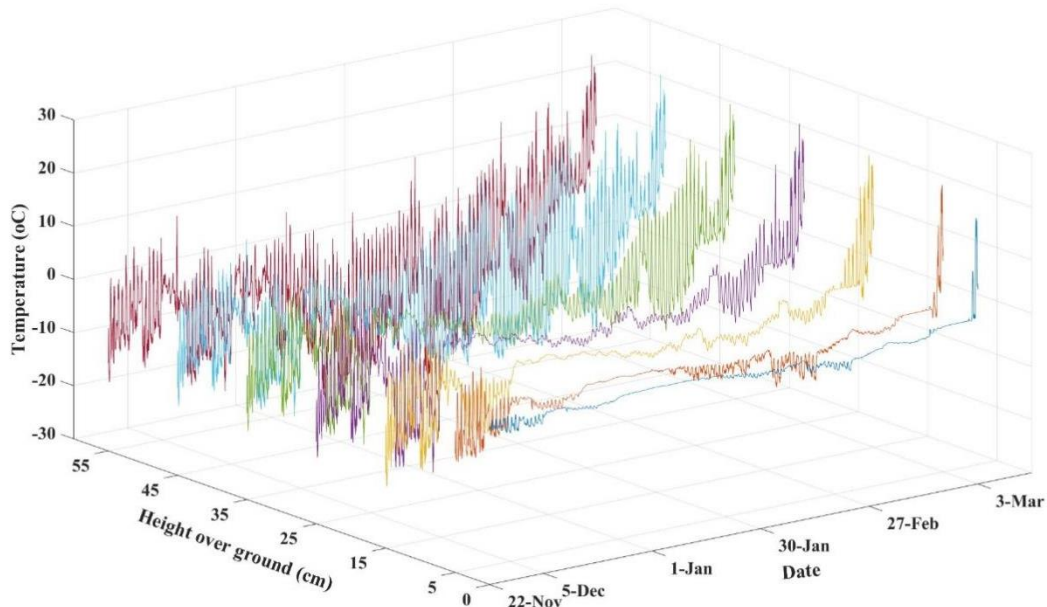
Figure 9. Daily variation in snow densities measured using three different measurement methods from November 27, 2015 to March 25, 2016, (a) overall snow density measured using snow tube, (b) snow density at 10-cm interval using snow shovel, and (c) snow density at 5-cm interval using snow fork.

337

338

339 **4.1.3 Snow temperature**

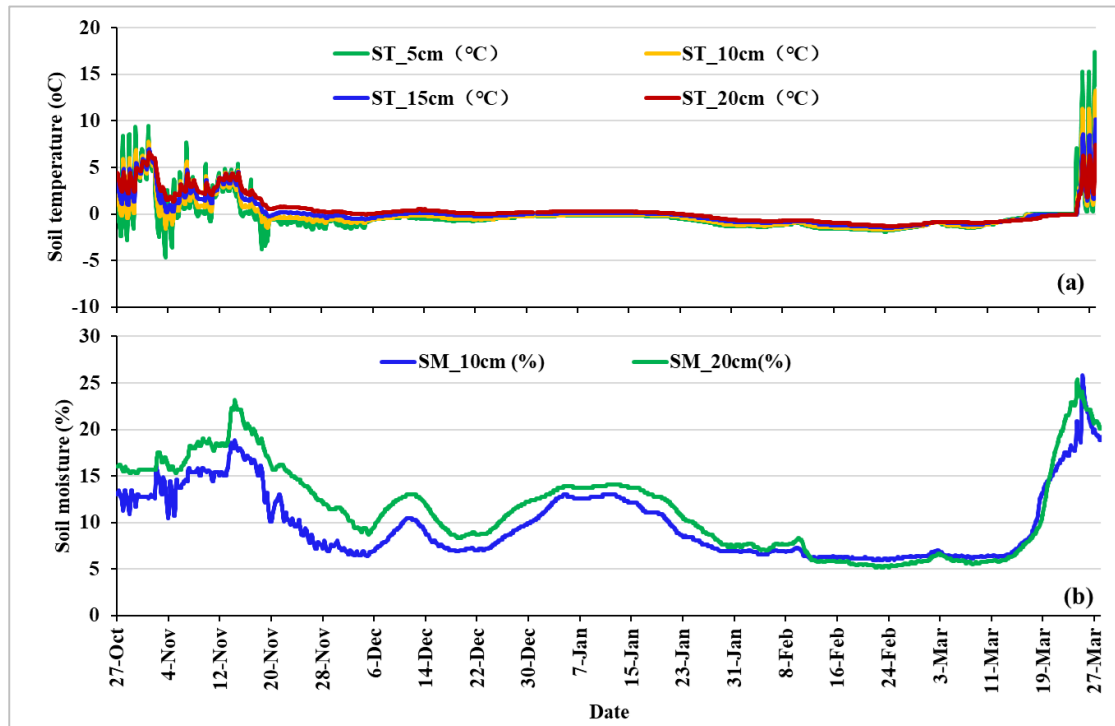
340 The diurnal range of snow temperature decreased from top to bottom layers. As the snow depth  
341 increased, there were more layers with small diurnal variations (Figure 10). Snow temperature at 0 cm  
342 (snow/soil interface temperature) showed no significant diurnal variation, remaining at approximately -  
343 2.0 to 0.7 °C. Snow temperature in the top layer had the largest diurnal variation. After March 17, 2016,  
344 the snow temperature of all layers were over 0°C, implying that snow cover did not refreeze anymore.



345 **Figure 10. Minutely variation in snow temperatures at 0 cm (snow/soil interface), 5 cm, 15 cm, 25 cm, 35 cm,**  
346 **45 cm and 55 cm above ground during experiment period**  
347

348 **4.2 Soil temperature and moisture**

349 The soil temperature at 5 and 10 cm remained stable and below 0 °C during the snow season but  
350 presented large fluctuation before (after) snow on (off) (Figure 11). The temperature difference between  
351 5 cm and 10 cm was much larger before snow cover onset than during snow cover period. The soil  
352 moisture at 10 cm were above 10% before snow cover onset and after snow off. There were two soil  
353 moisture peaks within the snow cover period, one from December 12-14 and the other from January 1-  
354 20.



355

356

357

Figure 11. (a) Hourly soil temperature at 5 cm, 10 cm, 15 cm and 20 cm below the snow/soil interface (a), and (b) soil moisture at 10 cm and 20 cm below the snow/soil interface.

358

### 4.3 Brightness temperature

359

360

361

362

363

364

365

366

367

368

369

370

The microwave brightness temperatures varied with snow, soil, and weather conditions. Figure 12 shows the daily brightness temperatures, brightness temperature difference between 18 and 36 GHz, and snow depth at 1:00 am local time. Figure 13 shows the hourly variation in brightness temperatures at 1.4 GHz, 18.7 GHz and 36.5 GHz and air temperature after February 1. Data show that Tb36h and Tb36v decreased during the full snow season, Tb18h exhibited an obvious decline after February 18, and Tb18v after March 3 (Figure 12). After January 4, though snow depth stopped increasing, the brightness temperature continued to decrease and brightness temperature difference increased. Based on Figure 8, snow density became stable after January 15. Therefore, after January 4, the decreasing brightness temperatures was mainly caused by growing grain size. The variation of L band mainly relies on soil moisture and soil temperature change. We have soil temperatures at 0 cm, 5 cm and 10 cm and soil moisture at 10 cm. However, the L band reflects the soil moisture within 5 cm which was absent in this experiment.

371

372

373

374

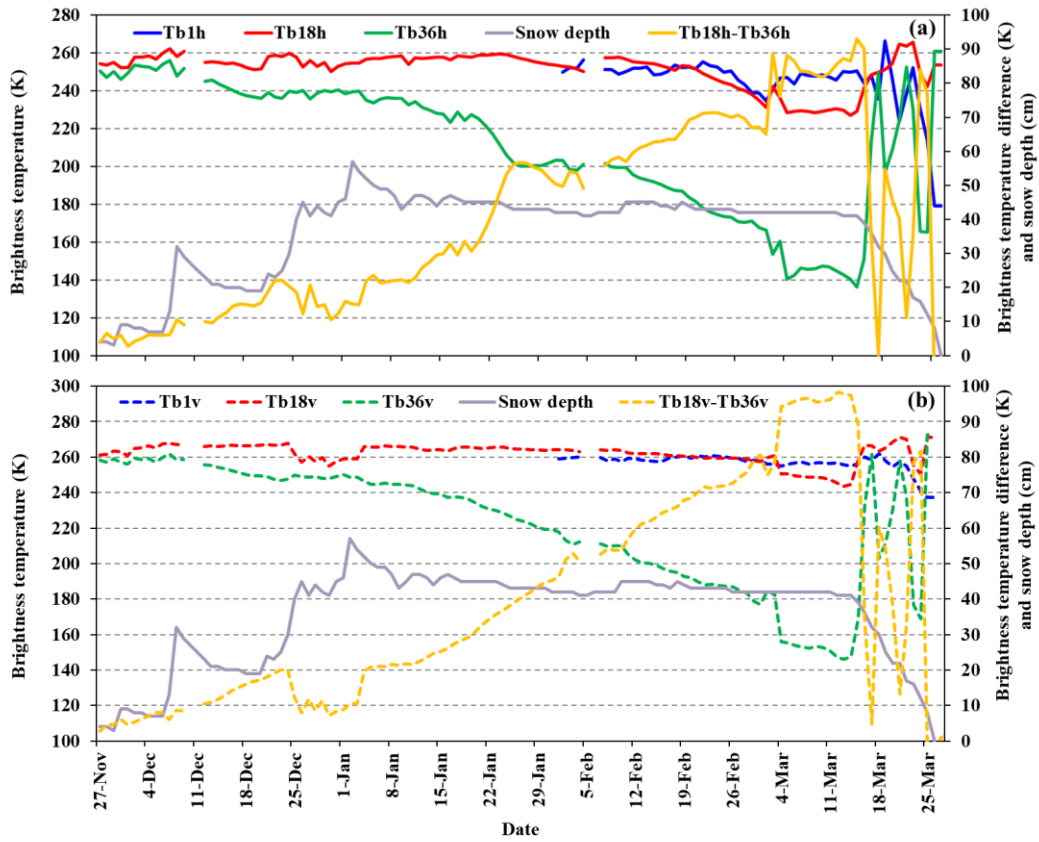
375

376

377

378

After February 25, brightness temperature exhibited a distinct cycle of daytime increase and nighttime decrease (Figure 13), resulting from large liquid water content caused by high daytime air temperature (above 0 °C) and the melted snowpack refreezing at nighttime. After March 14, there was another big rise in air temperature and even the nighttime air temperatures were above 0°C. During this period of accelerated snowmelt, as the liquid water within the snowpack did not refreeze completely at night, both brightness temperatures at three bands and brightness temperature difference exhibited irregular behavior.



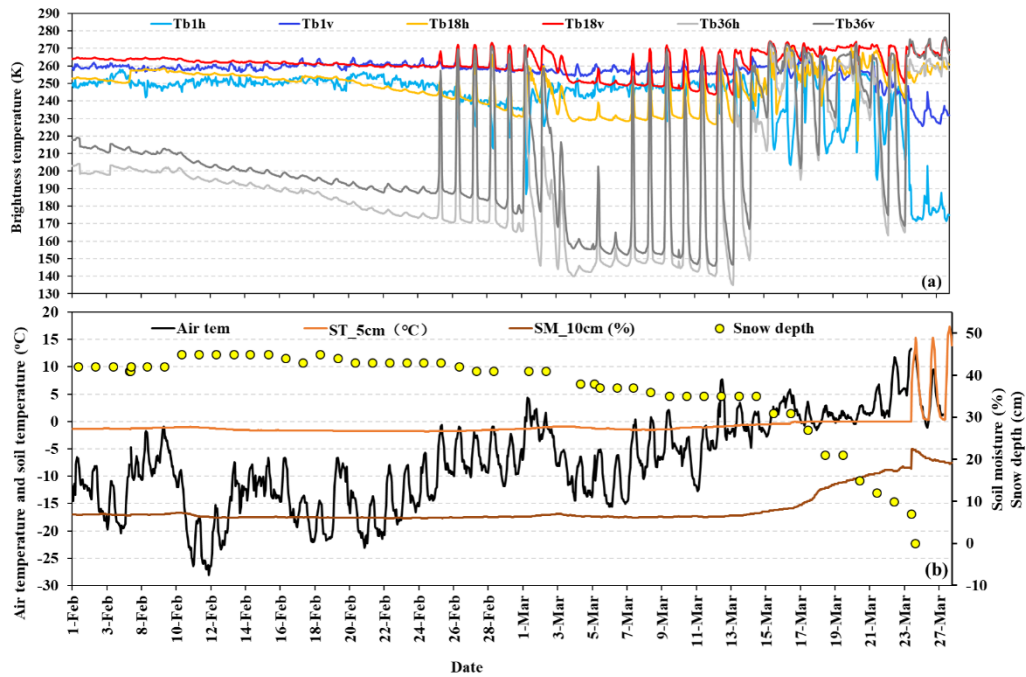
380

381 **Figure 12. Daily variations in brightness temperatures at 1.4 GHz, 18 GHz and 36 GHz, for horizontal**  
 382 **(Tb1h, Tb18h, Tb36h) and vertical polarizations (Tb1v, Tb18v, Tb36v), the differences between Tb18h and**  
 383 **Tb36h (Tb18h - Tb36h), and between Tb18v and Tb36v (Tb18v - Tb36v), at 1:00 am local time, from**  
 384 **November 27, 2015 to March 26, 2016. (a) for horizontal polarization, and (b) for vertical polarization.**

385

386

387



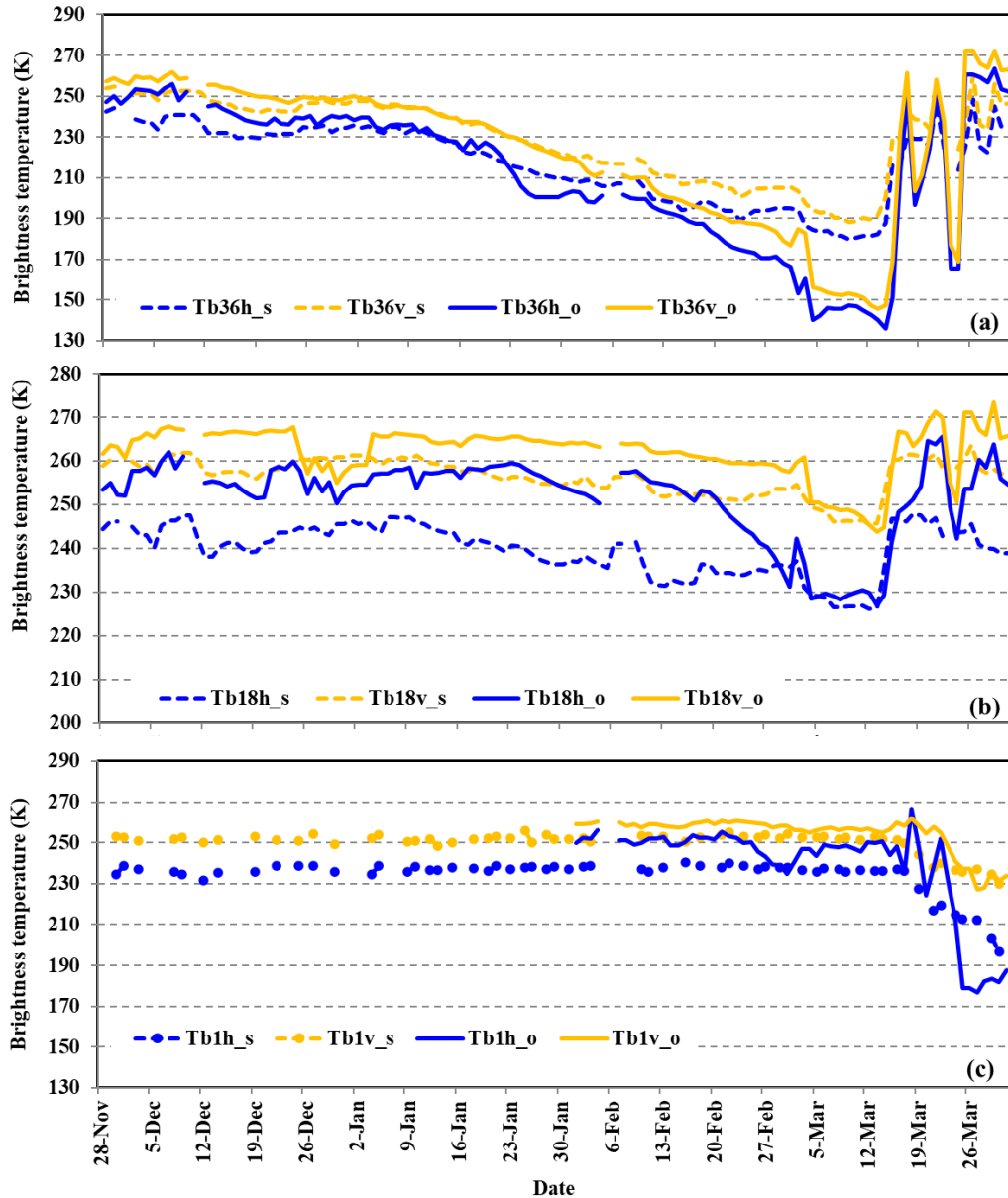
388

389 **Figure 13. Hourly variation in (a) Tb1h, Tb18h, Tb36h, Tb1v, Tb18v, and Tb36v, and (b) air temperature,**  
 390 **soil moisture at 10 cm and soil temperature at 5 cm, and daily variation in snow depth, from February 1 to**  
 391 **March 28, 2016.**

392

393 The brightness temperatures at 18.7 and 36.5 GHz from AMSR-2 and at 1.4 GHz from SMAP were  
 394 compared with the ground-based observations at the overpass time (Figure 14). Although there were  
 395 large differences between satellite and ground-based observations, the general temporal patterns were  
 396 the same. Specifically, the abrupt changes at 18.7 and 36.5 GHz on March 3 and March 16 were captured  
 397 by both satellites and ground-based sensors. Brightness temperatures at 1.4 GHz from both SMAP and  
 398 ground microwave radiometer kept stable before March 16, after when, brightness temperature rapidly  
 399 decreased because of the increase of soil moisture. The correlation coefficients at both polarizations were  
 400 approximately 0.96, 0.7 and 0.88 for 36.5 GHz, 18.7 GHz and 1.4 GHz, respectively. Satellite observed  
 401 brightness temperature presented less decrease trend than ground-based observation. The difference at  
 402 36.5 GHz is larger than those at 18.7 and 1.4 GHz. The difference between ground-based and satellite  
 403 observation might be attributed to the different field of views.

404



405

406

407

Figure 14. Comparison of brightness temperature between ground-based (o) and satellite-based observations (s), (a) for 36 GHz, (b) for 18 GHz, and (c) for 1.4 GHz.

408

#### 4.4 4-component Radiation

409

410

411

412

413

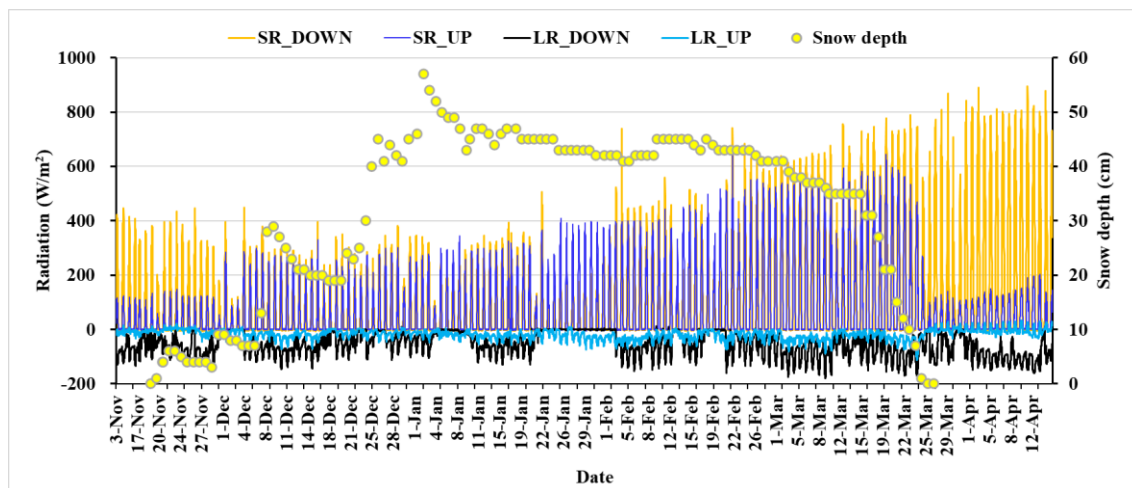
414

415

416

The land surface albedo is strongly related to the land cover. In this experiment, the downward short-wave radiation presented general increase after January, while the trend became distinctive after February (Figure 15). The upward short-wave radiation abruptly increased when the ground was covered by snow (after November 21), and sharply declined on the snow off day (March 25). From the first snowfall by the end of January, the ratios between upward and downward short-wave radiation were approximately 95%. The ratio decreased with snow age, and in the end of snow season, the ratios decreased to approximately 25% on snow off day.





417

418

Figure 15. Minutely variation in 4-component radiation and daily variation in snow depth at Altay station from November 3, 2015 to April 15, 2016.

419

420

## 5 Discussion

421

### 5.1 Applications

422

Our dataset is, though for one snow season, provides daily snow pit observations with coincident microwave and optical radiation data, including comprehensive and detailed snow parameters, allowing researchers to find more details in snow characteristics and their relationship with remote sensing signatures. The dataset also fills the snow observation gap in mid-low snow depth area with relative short snow cover duration.

423

424

425

426

427

The snow pit data and microwave brightness temperatures have proven useful for evaluating and updating a microwave emission transfer model of snowpack (Dai et al., 2022). This dataset reflected a general fact that brightness temperature at higher frequencies presented stronger volume scattering of snow grains, and were more sensitive to snow characteristics. This experiment revealed that the dominant control for the variation of brightness temperature was the variation of grain size but not snow depth or SWE. In the stable period, brightness temperature difference between 18.7 and 36.5 GHz increased with growing grain size in the condition of dry snowpack. Therefore, the daily snow depth variations curve derived from passive microwave remote sensing datasets tend to exhibit a temporal offset from those of in situ observation.

428

429

430

431

432

433

434

435

436

437

438

439

440

441

442

443

444

445

446

During the snow season, brightness temperatures for both polarizations presented similar variation trends, though behaving different in fluctuation. The horizontal polarization was more sensitive to environment and was less stable than vertical polarization. Besides, the polarization difference at 18.7 GHz and 36.5 GHz showed increase and decrease trends, respectively, during the experimental period. This phenomenon was different from the simulation results (Dai et al., 2022). The different polarization behavior at 18.7 and 36.5 GHz might be related to the environmental conditions, snow characteristics and soil conditions. However, as the subsurface soil moisture was not observed, the dynamic ground emissivity could not be estimated. As it is known, as L band has strong penetrability, the brightness temperature variations were predominantly related to subsurface soil conditions, unless for the situations that the liquid water content within snowpack was high. Therefore, in the condition of soil moisture data absence, L band brightness temperatures were expected to reflect soil moisture variation that influences the soil transmissivity (Babaeian et al., 2019; Naderpour et al., 2017; Hirahara et al., 2020).

448 Snow surface albedo significantly influences the incoming solar radiation, playing an important role  
449 in the climate system. The factors altering snow surface albedo contain the snow characteristics (grain  
450 size, SWE, liquid water content, impurities, surface temperature etc), external atmospheric condition and  
451 solar zenith angle (Aoki et al., 2003). Snow albedo was estimated based on snow surface temperatures  
452 in some models (Roesch et al., 1999), while others considered that snow surface albedo was mainly  
453 related to snow age (Mabuchi et al., 1997). In this experiment, we obtained the 4-component radiation,  
454 snow pit and meteorological data, providing nearly all observations of possible influence factors,  
455 therefore could be utilized to analyze shortwave radiation process of snowpack, and validate or improve  
456 multiple-snow-layer albedo models.

457 Snow grain sizes and snow densities within different layers presented different growth rates during  
458 different periods. Generally, the growth rates are related to the air temperature, pressure and snow depth  
459 (Chen et al., 2020; Essery, 2015; Vionnet et al., 2012; Lehning et al., 2002); therefore, this dataset can  
460 be used to analyze the evolution process of snow characteristics, as well as validation data for snow  
461 models.

## 462 5.2 Uncertainties

463 During the experiment, some uncertainties were produced due to irresistible factors. It was reported  
464 that the sampling depth of the L-band microwave emission under frozen and thawed soil conditions is  
465 determined at 2.5 cm (Zheng et al., 2019). We did not collect subsurface soil moisture, and the L band  
466 radiometer observation began on January 30, 2016. Therefore, it is difficult to obtain the ground  
467 emissivity in the full snow season based on the data. The soil moisture data at 10 and 20 cm under  
468 soil/snow interface cannot be directly used to validate and develop soil moisture retrieval from L band  
469 brightness temperature. In the future, detailed soil moisture profile will be observed to estimate the  
470 subsurface soil moisture to fill the gap.

471 The grain size data were collected through taking photos. When measuring the length of grains, the  
472 grain selection has subjectivity, and the released data are statistic results based on the recorded grain  
473 sizes. Although the general variation trend can be reflected by the time series of average grain size, some  
474 details might be missed. Therefore, for who with interests, the original grain photos could be provided  
475 through requesting for authors. In snowmelt period, large liquid water content would influence the  
476 measurement results of snow fork. Therefore, it is suggested to use small-size snow shovel or cutter to  
477 observe layered snow density in future experiments.

478 One season observation is quite valuable for developing and validate remote sensing snow retrieval  
479 method or snow model, although the representativeness of this observation requires further analysis.  
480 Nevertheless, more years of observations should be considered to increase the statistical significance of  
481 the evolution of snow characteristics.

## 482 6 Conclusions

483 In a summary, the IMCS campaign provides snow pits observation, meteorological parameters,  
484 optical radiation and passive microwave brightness temperatures in the snow season of 2015/2016. The  
485 dataset is unique in providing microwave brightness temperatures and coincident daily snow pits data  
486 over a full snow season at a fix site. The first use of our dataset is for the validation of snow microwave  
487 emission models, improving its simulation accuracy.

488 The daily snow pit data provide snow grain size, grain shape, snow density and snow temperature  
489 profiles. Generally, grain size grew with snow age, and increased from top to bottom. Snow grains are

490 rounded shape with small grain size in the top layer, and depth hoar with large grain size in the bottom  
491 layer. Snow density experienced increase-stable-increase variation, and the densities of the middle layers  
492 were greater than the bottom layer due to the well-developed depth hoar in the stable period. The data  
493 can be used to analyze the evolution process of snow characteristics combining with weather data, also  
494 for the validation and improvement of the snow process models, such as SNOWPACK (Lehning et al.,  
495 2002), SNTherm (Chen et al., 2020), etc. The improvement of these snow process models can further  
496 enhance the prediction accuracy of land surface process and hydrology models.

497 Microwave radiometer data and snow pit data have been utilized to analyze the volume scattering  
498 features of snowpack at different frequencies (Dai et al., 2022). Results showed that grain size was the  
499 most important factor to influence snow volume scattering. The data can also be used for analysis of  
500 polarization characteristics of snowpack, combining with soil and weather data.

501 The microwave and optical radiations were simultaneously observed. Existing studies reported that  
502 the optical equivalent diameter must be used in microwave emission model with caution (Löwe and  
503 Picard, 2015; Roy et al., 2013). These data provide a new opportunity to analyze the difference between  
504 the influence of grain size on microwave and optical radiation, establishing the bridge between effective  
505 optical grain size and microwave grain size.

## 506 **7 Data availability**

507 The IMCS consolidated datasets are available on the National Tibetan Plateau Data Center and  
508 available online at <http://data.tpsc.ac.cn/zh-hans/data/df1b5edb-daf7-421f-b326-cdb278547eb5/> (doi:  
509 10.11888/Snow.tpsc.270886). Microwave radiometry raw Data are available for scientific use on request  
510 from Northwest Institute of Eco-Environment and Resources, Chinese Academy of Sciences.

511  
512

513 **Author contributions:** LD and TC designed the experiment. LD, YZ, JT, MA, LX, SZ, YY YH and LX  
514 collected the passive microwave and snow pit data. HL provided the 4-component radiation and snow  
515 temperature data. LW provided meteorological data. LD write the manuscript, and TC made revision. All  
516 authors contributed to the data consolidation.

517

518 **Competing interests:** The authors declare that they have no conflict of interest.

519

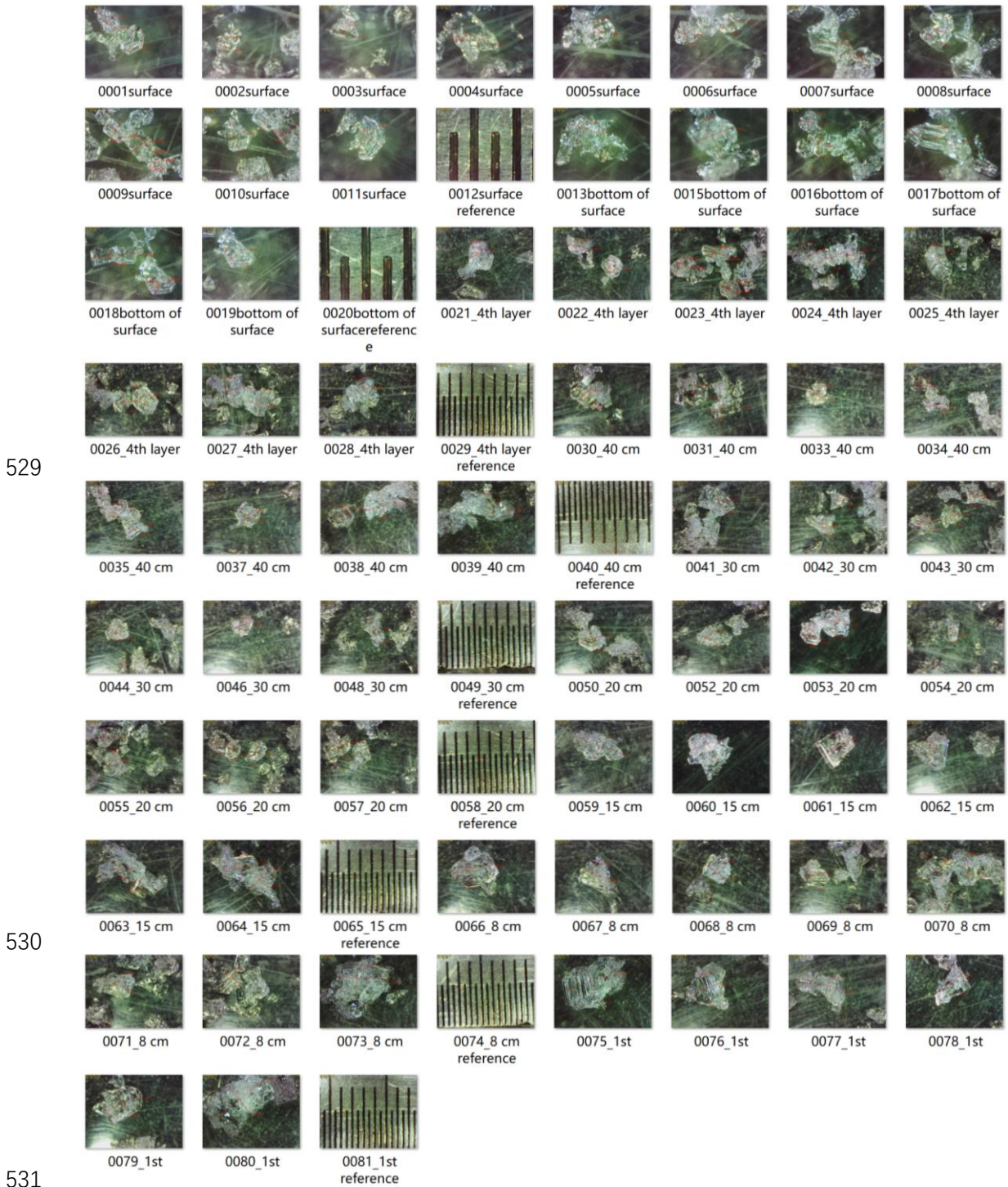
520 **Acknowledgment:** The authors would like to thank the Altay meteorological station for providing  
521 logistics service and meteorological data.

522

523 **Financial support:** This research was funded by the National Science Fund for Distinguished Young  
524 Scholars (grant nos: 42125604), National Natural Science Foundation of China (grant nos: 42171143),  
525 and CAS 'Light of West China' Program.

526

527



529

530

531

532

533 **Figure A1. Photos of grains and reference ruler in each layer on February 15, 2016. In each photo the**

534 **longest and shortest axis lengths of the chosen grains are labeled. Original photos are in URL:**

535 **<http://arcticroute.tpdc.ac.cn/navigate/bmp>**

536

537

538

539

540

**Table A1. Recorded longest and shortest axis length in Figure A.**

Stratigraphy	Thickness (cm)	Shape	Grain size (longest axis * shortest axis)(mm)								
the fifth	3cm	#22	0.595 *0.43 6	0.472 *0.47 1	0.450 *0.43 6	0.615 *0.47 4	0.374 *0.31 4	0.647 *0.30 7	0.656 *0.52 9	0.544 *0.51 9	0.717 *0.44 7
			0.750 *0.44 5	1.056 *0.95 5	0.623 *0.37 8	0.451 *0.40 5	1.397 *0.63 5	1.235 *0.32 7	0.600 *0.42 1	0.633 *0.55 6	0.729 *0.42 3
the fourth	3cm	#37	2.605 *2.01 1	1.850 *1.32 8	1.626 *1.55 4	1.767 *1.68 5	1.718 *1.53 5	2.255 *1.29 6	1.674 *1.60 1	1.542 *1.26 9	3.505 *1.44 0
			3.055 *1.77 4	1.448 *1.37	2.461 *1.91 4	2.757 *2.11 5	2.179 *2.05 9	2.393 *1.78 8			
the third	25cm	#27, #31, #37	2.569 *1.60 7	2.073 *2.13 0	2.591 *1.41 4	1.869 *1.80 2	2.067 *1.26 6	1.209 *1.10 6	1.719 *1.18 8	1.648 *0.97 5	1.911 *1.58 2
			1.921 *1.71 0	1.518 *1.06 7	1.291 *1.14 7	1.690 *1.55 1	1.756 *1.39 8	1.812 *1.26 3	1.733 *1.67 2	1.880 *1.51 8	2.411 *1.22 0
			2.118 *1.72 7	1.614 *1.45 7	1.795 *1.70 5	2.215 *2.31 1	1.864 *1.69 2	1.967 *1.65 1	2.008 *1.39 5	1.362 *1.14 1	1.484 *1.29 1
the second	12	#33, #34	4.251 *2.26 6	3.012 *2.65	2.805 *1.99 5	1.799 *1.41 5	1.402 *1.19 5	3.040 *2.07 3	2.850 *2.09 5		
			3.900 *2.53 2	2.420 *2.33 3	2.515 *2.20 6	2.044 *2.03 2	2.506 *2.36 3	2.894 *2.16 1	2.413 *1.95 0	2.494 *1.81 6	4.929 *3.25 7
the first	4	#40, #34, #38	4.933 *3.37 8	3.207 *2.77 4	3.562 *1.70 1	2.818 *1.66 8	3.581 *2.51 8	6.179 *3.56 2			

541

542

**Table A2. An example of record table for snow density observation.**

543

observation date: 20160111		observation time: 9:03-9:40		weather: clear		snow depth: 48cm	
Snow Fork table				Snow tube table			
observation height (cm)	liquid water content(%)	snow density (g/cm <sup>3</sup> )	snow depth(cm)				
5	0	0.1923	46.5		47		47.5
	0.118	0.1882	snow pressure(g/cm <sup>2</sup> )	9.1	9		9.5
	0	0.1882	snow density(g/cm <sup>3</sup> )	0.1957	0.1915		0.2000
10	0.461	0.164	snow shovel table				
	0.46	0.1631					
	0.461	0.1361					
15	0.123	0.2532	observation layer (cm)	weight of shovel+snow(g)	weight of shovel(g)	snow density(g/cm <sup>3</sup> )	
	0	0.2506	0-10	865.04	572.16	0.1953	
	0	0.2417		858.72	572.16	0.1910	
0.24	0.2159	866.69		572.16	0.1964		
20	0.119	0.2155	10-20	878.58	572.16	0.2043	
	0.119	0.2146		887.04	572.16	0.2099	
	0.117	0.1977		872.79	572.16	0.2004	
25	0	0.1994	20-30	905.34	572.16	0.2221	
	0	0.1984		903.41	572.16	0.2208	
	0	0.1919		907.88	572.16	0.2238	
30	0	0.1966	30-40	832.75	572.16	0.1737	
	0	0.1928		838.14	572.16	0.1773	
	0	0.1534		837.27	572.16	0.1767	
35	0	0.1517	40-50				
	0	0.1472					
	0.325	0.1097					
40	0	0.1054	50-60				
	0.107	0.1088					
	0	0.0922					
45	0	0.0991					
	0	0.0928					
50							

544  
545  
546

547 **References:**

548 Aoki, T., Hachikubo, A., and Hori, M.: Effects of snow physical parameters on shortwave broadband  
549 albedos, *J. Geophys. Res-Atmos.*, 108 (D19), 4616, <https://doi.org/10.1029/2003JD003506>, 2003.

550 Babaeian, E., Sadeghi, M., Jones, S.B., Montzka, C., Vereecken, H., and Tuller, M.: Ground, Proximal,  
551 and Satellite Remote Sensing of Soil Moisture, *Rev. Geophys.*, 57(2), 530-616, [https://doi.org/](https://doi.org/10.1029/2018RG000618)  
552 10.1029/2018RG000618, 2019.

553 Brucker, L., Hiemstra, C., Marshall, H.-P., Elder, K., De Roo, R., Mousavi, M., Bliven, F., Peterson,  
554 W., Deems, J., Gadowski, P., Gelvin, A., Spaete, L., Barnhart, T., Brandt, T., Burkhart, J., Crawford,  
555 C., Datta, T., Erikstrod, H., Glenn, N., Hale, K., Holben, B., Houser, P., Jennings, K., Kelly, R., Kraft,  
556 J., Langlois, A., McGrath, D., Merriman, C., Molotch, N., Nolin, A., Polashenski, C., Raleigh, M.,  
557 Rittger, K., Rodriguez, C., Roy, A., Skiles, M., Small, E., Tedesco, M., Tennant, C., Thompson, A.,  
558 Tian, L., Uhlmann, Z., Webb, R., and Wingo, M.: A first overview of snowex ground-based remote  
559 sensing activities during the winter 2016-2017, *Int. Geosci. Remote Sen.*, 1391-1394,  
560 <http://dx.doi.org/10.1109/IGARSS.2017.8127223>, 2017.

561 Chen, T., Pan, J.M., Chang, S.L., Xiong, C., Shi, J.C., Liu, M.Y., Che, T., Wang, L.F., and Liu, H.R.:  
562 Validation of the SNTHERM Model Applied for snow depth, grain size, and brightness temperature  
563 simulation at meteorological stations in China, *Remote Sens.*, 12, 507, [https://doi.org/Artn](https://doi.org/Artn50710.3390/Rs12030507)  
564 50710.3390/Rs12030507, 2020.

565 Cline, D., Elder, K., Davis, B., Hardy, J., Liston, G., Imel, D., Yueh, S., Gasiewski, A., Koh, G.,  
566 Armstrong, R., and Parsons, M.: An overview of the NASA Cold Land Processes Field Experiment  
567 (CLPX-2002), *P. Soc. Photo-Opt. Ins.*, 4894, 361-372, [https://doi.org/ 10.1117/12.467766](https://doi.org/10.1117/12.467766), 2003.

568 Dai, L.: Microwave radiometry experiment data in Altay (2015/2016), National Tibetan Plateau Data  
569 Center [dataset], <https://doi.org/10.11888/Snow.tpcd.270886>, 2020.

570 Dai, L.Y., Che, T., Xiao, L., Akynbekkyzy, M., Zhao, K., and Leppänen, L.: Improving the Snow  
571 Volume Scattering Algorithm in a Microwave Forward Model by Using Ground-Based Remote



572 Sensing Snow Observations, *Ieee T. Geosci. Remote.*, 60, 4300617,  
573 <https://doi.org/10.1109/TGRS.2021.3064309>, 2022.

574 Derksen, C., Toose, P., Lemmetyinen, J., Pulliainen, J., Langlois, A., Rutter, N., and Fuller, M.C.:  
575 Evaluation of passive microwave brightness temperature simulations and snow water equivalent  
576 retrievals through a winter season, *Remote Sens. Environ.*, 117, 236-248, [https://doi.org/](https://doi.org/10.1016/j.rse.2011.09.021)  
577 [10.1016/j.rse.2011.09.021](https://doi.org/10.1016/j.rse.2011.09.021), 2012.

578 Essery, R.: A factorial snowpack model (FSM 1.0), *Geosci. Model Dev.* 8, 3867–3876,  
579 <https://doi.org/10.5194/gmd-8-3867-2015>, 2015.

580 Fierz, C., Armstrong, R.L., Durand, Y., Etchevers, P., Greene, E., McClung, D.M., Nishimura, K.,  
581 Satyawali, P.K. and Sokratov, S.A.: The International Classification for Seasonal Snow on the Ground.  
582 IHP-VII Technical Documents in Hydrology N<sup>o</sup>83, IACS Contribution N<sup>o</sup>1, UNESCO-IHP, Paris,  
583 2009.

584 Hirahara, Y., de Rosnay, P., and Arduini, G.: Evaluation of a microwave emissivity module for snow  
585 covered area with CMEM in the ECMWF Integrated Forecasting System, *Remote Sens.*, 12(18),  
586 <https://doi.org/10.3390/rs12182946>, 2020.

587 Lehning, M., Bartelt, P., Brown, B., Fierz, C., and Satyawali, P.: A physical SNOWPACK model for  
588 the Swiss avalanche warning Part II: Snow microstructure, *Cold Reg. Sci. Technol.*, 35, 147-167,  
589 [https://doi.org/10.1016/S0165-232x\(02\)00073-3](https://doi.org/10.1016/S0165-232x(02)00073-3), 2002.

590 Lemmetyinen, J., Kontu, A., Pulliainen, J., Vehvilainen, J., Rautiainen, K., Wiesmann, A., Matzler, C.,  
591 Werner, C., Rott, H., Nagler, T., Schneebeli, M., Proksch, M., Schuttemeyer, D., Kern, M., and  
592 Davidson, M.W.J.: Nordic Snow Radar Experiment, *Geosci. Instrum. Meth.*, 5, 403-415,  
593 <https://doi.org/10.5194/gi-5-403-2016>, 2016.

594 Li, X., Che, T., Li, X. W., Wang, L., Duan, A. M., Shangguan, D. H., Pan, X. D., Fang, M. and Bao,  
595 Q.: CASEarth Poles Big Data for the Three Poles, *B. Am. Meteorol. Soc.*, 101(9): E1475-E1491,  
596 <https://doi.org/10.1175/Bams-D-19-0280.1>, 2020.

597 Löwe, H. and Picard, G.: Microwave scattering coefficient of snow in MEMLS and DMRT-ML  
598 revisited: The relevance of sticky hard spheres and tomography-based estimates of stickiness,  
599 *Cryosphere*, 9(6), 2101–2117, <https://doi.org/10.5194/tc-9-2101-2015>, 2015.

600 Mabuchi, K., Sato, Y., Kida, H., Saigusa, N. and Oikawa, T.: A biosphere-atmosphere interaction  
601 model (BAIM) and its primary verification using grassland data, *Pap. Meteorol. Geophys.*, 47, 115–  
602 140, <https://doi.org/10.2467/mripapers.47.115>, 1997.

603 Naderpour, R., Schwank, M., Matzler, C., Lemmetyinen, J., and Steffen, K.: Snow Density and Ground  
604 Permittivity Retrieved From L-Band Radiometry: A Retrieval Sensitivity Analysis. *Ieee J-Stars.*, 10(7),  
605 3148-3161, <https://doi.org/10.1109/Jstars.2017.2669336>, 2017.

606 Pan, X. D., Guo, X. J., Li, X., Niu, X. L., Yang, X. J., Feng, M., Che, T., Jin, R., Ran, Y. H., Guo, J.  
607 W., Hu, X. L. and Wu, A. D.: National Tibetan Plateau Data Center Promoting Earth System Science  
608 on the Third Pole, *B. Am. Meteorol. Soc.*, 102(11), E2062-E78, <https://doi.org/Bams-D-21-0004.1>,  
609 2021.

610 Roesch, A., Gilgen, H., Wild, M., and Ohmura, A.: Assessment of GCM simulated snow albedo using  
611 direct observations, *Clim. Dynam.*, 15, 405–418, <https://doi.org/10.1007/s003820050290>, 1999.

612 Roy, A., Picard, G., Royer, A., Montpetit, B., Dupont, F., Langlois, A., Derksen, C., and Champollion,  
613 N.: Brightness Temperature Simulations of the Canadian seasonal snowpack driven by measurements  
614 of the snow specific surface area, *Ieee T. Geosci. Remote.*, 51, 4692-4704,  
615 <https://doi.org/10.1109/Tgrs.2012.2235842>, 2013.

616 Royer, A., Roy, A., Montpetit, B., Saint-Jean-Rondeau, O., Picard, G., Brucker, L., and Langlois, A.:  
617 Comparison of commonly-used microwave radiative transfer models for snow remote sensing, *Remote*  
618 *Sens. Environ.*, 190, 247-259, <https://doi.org/10.1016/j.rse.2016.12.020>, 2017.

619 Tedesco, M., and Kim, E.J.: Intercomparison of electromagnetic models for passive microwave remote  
620 sensing of snow, *Ieee T. Geosci. Remote.*, 44, 2654-2666, <https://doi.org/10.1109/TGRS.2006.873182>,  
621 2006.

622 Vionnet, V., Brun, E., Morin, S., Boone, A., Faroux, S., Le Moigne, P., Martin, E., and Willemet, J.M.:  
623 The detailed snowpack scheme Crocus and its implementation in SURFEX v7.2, *Geosci. Model Dev.*,  
624 5, 773-791, <https://doi.org/10.5194/gmd-5-773-2012>, 2012.

625 Zheng, D., Li, X., Zhao, T., Wen, J., van der Velde, R., Schwank, M., Wang, X., Wang, Z., and Su, Z.:  
626 Impact of soil permittivity and temperature profile on L-Band microwave emission of frozen soil. *Ieee*  
627 *T. Geosci. Remote.*, 59(5), 4080-4093, <https://doi.org/10.1109/TGRS.2020.3024971>, 2021.

628 Zhang, P., Zheng, D., van der Velde, R., Wen, J., Zeng, Y., Wang, X., Wang, Z., Chen, J., and Su, Z.:  
629 Status of the Tibetan Plateau observatory (Tibet-Obs) and a 10-year (2009–2019) surface soil moisture  
630 dataset, *Earth Syst. Sci. Data*, 13, 3075–3102, <https://doi.org/10.5194/essd-13-3075-2021>, 2021.

631 Zheng, D., Li, X., Wang, X., Wang, Z., Wen, J., van der Velde, R., Schwank, M., and Su, Z.: Sampling  
632 depth of L-band radiometer measurements of soil moisture and freeze-thaw dynamics on the Tibetan  
633 Plateau, *Remote Sens. Environ.*, 226, 16-25, <https://doi.org/10.1016/j.rse.2019.03.029>, 2019.